used for comparisons between the physiological states and p values <0.05 were considered significant.

The ROI for the whole region was divided plane-by-plane into subregions of ten pixels each. The subregions were created by extracting pixels first from the horizontal direction and then from the vertical direction inside the whole ROI in each slice. Each subregion consisted of a single area with the same number of pixels. Functional values of K_1, k_2 and V_A were extracted from each subregion. Tissue TACs were also obtained for each subregion from corresponding dynamic images. The three parameters K_1, k_2 and V_A were estimated using the Eq. 1 and the input function fitted to the tissue TACs by the nonlinear least-squares fitting method (NLF, Gauss-Newton method). Functional values of K_1, k_2 and V_A from corresponding subregions were then compared between the methods. Regression analysis was performed.

The model relevancy introducing p and/or V_A into the computation was tested using the Akaike Information Criterion (AIC) [20]. The most appropriate model provides the smallest AIC. The tissue TACs from the subregions were fitted and AICs were computed for models with the three parameters K_1, k_2 and V_A, fixing p ($=K_1/k_2$) at 0.35 ml/g (mean value obtained in the present subjects), fixing V_A at 0 ml/ml, and fixing V_A at 0.15 ml/ml (mean value obtained in the present subjects).

Error analysis in the simulation

Error propagation from errors in the input function for the present BFM formula was analysed for two factors: delay and dispersion in arterial TAC. It is known that the measured arterial TAC is delayed and more dispersed relative to the true input TAC in the kidney because of the time for transit of blood through the peripheral artery and the catheter tube before reaching the detector [18, 19]. Calculations of RBF so far have employed a fixed partition coefficient (p, $=K_1/k_2$, ml/g) and/or assumed the blood volume (V_A, ml/ml) as negligible throughout the whole renal region and do not estimate it regionally. BFM formulae with a fixed value of p (BFM-pfix) and blood volume V_A (BFM-vfix) in addition to the present BFM formula, and the error in these formulae, were analysed.

A typical arterial input function obtained from the present PET study was used in the present simulation as the true input function. Applying this input function to the water kinetic model in Eq. 1, a tissue TAC was created assuming values for normal kidney tissue (K_1=2.0 ml/min/g, V_A=0.14 ml/g [5], and p=0.4 ml/g, corresponding to the estimated means in cortical region in all subjects in this study).

Time in the input function was shifted from −4 to 4 s to simulate the error sensitivity due to the error in the time delay, where a positive error represents an over-correction of the time delay. The input function was convoluted or deconvoluted with a simple exponential [18] by shifting the time constant from −4 to 4 s to simulate the error sensitivity due to error in dispersion correction, where a negative error represents under-correction, as described previously [18, 21]. Values of K_1 and k_2 were calculated using simulated input functions and the tissue TACs based on the BFM formula. Errors in these calculated K_1 and k_2 values are presented as percentage differences from the assumed values. Then, the value of p was varied from 0.3 to 0.5 ml/g and the tissue TAC was generated as above to simulate the error from the value of p in BFM-pfix formula. Also, the V_A value was varied from 0.0 to 0.4 ml/ml and the tissue TAC was generated to simulating the error from V_A in BFM-vfix formula. Then, K_1 and k_2 were calculated using the true input function and the created tissue TACs, assuming p=0.4 ml/g and V_A=0.0 ml/ml in the BFM-pfix and BFM-vfix formulae, respectively. Error in K_1 and k_2 values due to fixing p is presented as the percentage difference in K_1 and k_2 as a function of p. Error in K_1 and k_2 values due to neglecting V_A is presented as the percentage difference in K_1 and k_2 as a function of V_A. Also, K_1 and k_2 were computed with V_A fixed at 0.14 ml/ml in the BFM-vfix formula from the set of the tissue TACs, in which K_1 and p were fixed at 2.0 ml/min/g and 0.4 ml/g, respectively, and V_A was varied. The percentage difference in K_1 and k_2 between the two conditions, i.e. the initial (K_1=2.0 ml/min/g and V_A=0.14 ml/ml) and changed conditions (presented as ΔK_1 and Δk_2, respectively) is presented as a function of the percentage difference in the assumed V_A from 0.14 ml/ml (ΔV) to investigate the extents to which the change in K_1 and k_2 were estimated when K_1 and k_2 were computed in the BFM-vfix formula.

Results

Experiments

The relationships of the regional ROI values of K_1, k_2 and V_A between NLF and BFM are shown in Fig. 2. The regression lines obtained were $K_{1,BFM}=0.93K_{1,NLF}-0.11$ ml/min/g (r=0.80, p<0.001), $k_{2,BFM}=0.96k_{2,NLF}-0.13$ ml/min/g (r=0.77, p<0.001), and $V_{A,BFM}=0.92V_{A,NLF}-0.00$ ml/ml (r=0.97, p<0.001), where the subscripts show the methods used for calculating the parametric values; the slopes were not significantly different from unity.

The fitted curve by the present model estimating K_1, k_2 and V_A fitted better than the other two models fixing p ($=K_1/k_2$) or V_A. An example of fitted curves is shown in Fig. 3. Also, the AIC values from three parameter fitting were the smallest for all subjects except two values for two

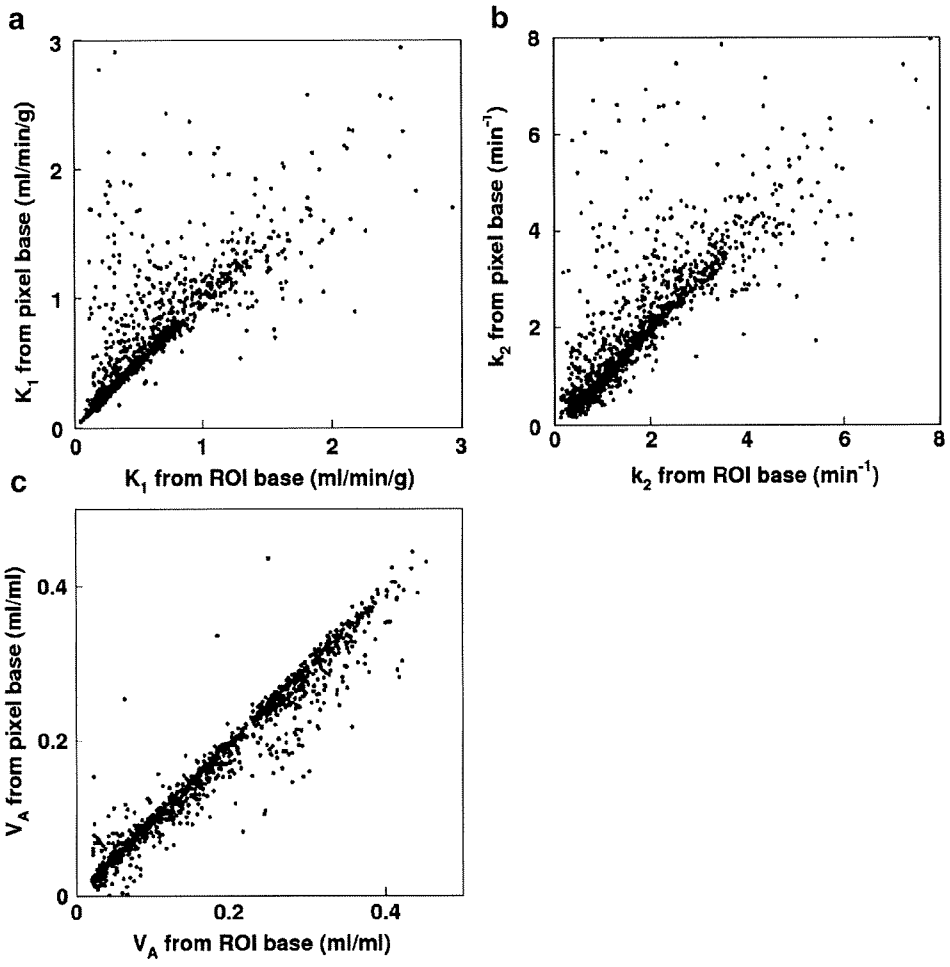

Fig. 2 Relationships of (**a**) K_1, (**b**) k_2 and (**c**) V_A between the ROI-based NLF method and pixel-based BFM. The regression lines were $K_{1,BFM}=0.93K_{1,NLF}-0.11$ ml/min/g ($r=0.80$, $p<0.001$), $k_{2,BFM}=0.96k_{2,NLF}-0.13$ ml/min/g ($r=0.77$, $p<0.001$), and $V_{A,BFM}=0.92V_{A,NLF}-0.00$ ml/ml ($r=0.97$, $p<0.001$)

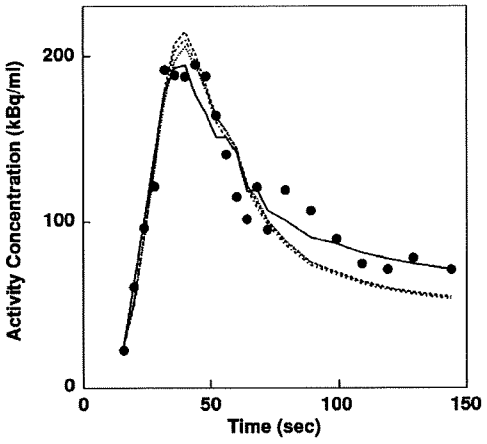

Fig. 3 Curves fitted to the measured tissue TAC from the different computation methods. Three parameters: K_1, k_2 and V_A were computed. p-fixed: K_1 and V_A were computed with p ($=K_1/k_2$) fixed at 0.35 ml/g. V_A-fixed: K_1 and k_2 were computed with V_A fixed at 0.15 ml/g. V_A-ignored: K_1 and k_2 were computed without taking into account V_A

parameter fitting fixing V_A in patient 2 and fixing p in patient 3, although some AIC values were similar (Table 2). These results show that the present method with three parameter fitting is feasible for computing RBF.

Values of K_1, $k_2 \cdot p_{phys}$ and V_A were obtained for the whole renal region and cortical region (Table 3). The K_1

Table 2 AIC values for the models

Subject	Three parameters[a]	p-fixed[b]	V_A-fixed (0.15)[c]	V_A-ignored[d]
1	484±20	519±28	499±15	494±15
2	474±9	486±14	474±9	477±8
3	525±12	523±8.3	527±10	527±7
4	483±14	497±21	501±12	506±13
5	497±18	502±19	508±32	499±13
6	496±11	507±14	500±9	497±9

[a] K_1 and k_2, V_A computed.
[b] K_1 and V_A computed with k_2 fixing such that $p=K_1/k_2=0.35$ ml/g.
[c] K_1 and k_2 computed with V_A fixed at 0.15 ml/g.
[d] K_1 and k_2 computed without taking into account V_A.

Table 3 Values of K_1, $k_2 \cdot p_{phys}$ and V_A (n=6) in the whole renal region and the cortical region calculated by the present method for the baseline conditions and the stimulated conditions

	K_1 (ml/min/g)	$k_2 \cdot p_{phys}$ (ml/min/g)	V_A (ml/ml)	GFR (ml/min/g)
Whole region				
Baseline	1.09±0.33	3.11±1.48	0.15±0.09	0.35±2[a]
Enalapril-stimulated	1.03±0.44	2.55±1.29	0.16±0.14	
Cortical region				
Baseline	1.57±0.60*	3.64±2.15*	0.18±0.12*	
Enalapril-stimulated	1.42±0.39*	3.55±1.64*	0.25±0.14*	

No significant difference was found between the baseline and stimulated conditions.
*Difference was significant between the whole and cortical regions.
[a] A kidney weight of 300 g and a cortex ratio of 70% were assumed.

values were smaller than $k_2 \cdot p_{phys}$ values and the ratio between them ranged from 0.35 to 0.45, suggesting that K_1 values underestimated RBF due to the partial volume effect. Both K_1 and $k_2 \cdot p_{phys}$ were not significantly different between the resting and stimulated conditions for the whole renal region and the cortical region, respectively, although the value of V_A was higher under the stimulated conditions than under the basal conditions. The GFR obtained was 78±4 ml/min, corresponding to a clearance rate of 0.37±0.02 ml/min/g and to 9.6% of the k_2 obtained for the cortical region under the normal conditions.

Representative K_1 and $k_2 \cdot p_{phys}$ images generated by the present method are shown in Fig. 4. The quality of the image is acceptable. The K_1 and $k_2 \cdot p_{phys}$ values ranged from 1.5 to 2.0 ml/min/g and 3.0 to 5.0 around cortical region, respectively, and some parts showed higher values than these. The average time required to compute the parametric images was 2 min 23 s.

Error analysis

The sizes of the errors introduced in both K_1 and k_2 were less than 20% for estimation of delay and the dispersion time constant up to 2 s (Fig. 5). The error sensitivity in K_1 and k_2 was 40% when the partition coefficient was 0.35 (Fig. 6). The magnitude of the error was markedly enhanced when the blood volume was ignored (Fig. 7a), and if the arterial blood volume increased by 25%, K_1 and k_2 were overestimated by 20% (Fig. 7a).

Discussion

We have presented an approach to generating quantitative K_1, k_2 and V_A images using $H_2{}^{15}O$ and PET applying the BFM computation method. The validity of this approach in healthy human subjects under resting and stimulated conditions is described. The rate constant values of K_1 and $k_2 \cdot p_{phys}$ obtained from the parametric images were consistent against NFL and the quality of the K_1 and $k_2 \cdot p_{phys}$ images obtained was acceptable. The smaller K_1 against $k_2 \cdot p_{phys}$ values suggested that the K_1 values underestimated the absolute RBF value due to the partial volume effect. The simulation showed that the delay time and dispersion time constant should be estimated within an accuracy of 2 s, and V_A and p cannot be ignored/fixed to

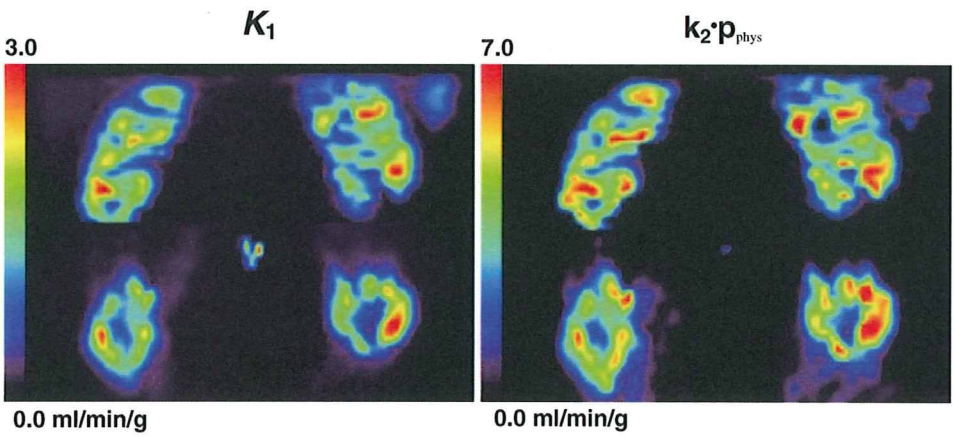

Fig. 4 Representative parametric images of K_1 (*left*) and $k_2 \cdot p_{phys}$ (*right*) for a subject under baseline conditions. Coronal (*upper*) and transverse (*lower*) views are shown

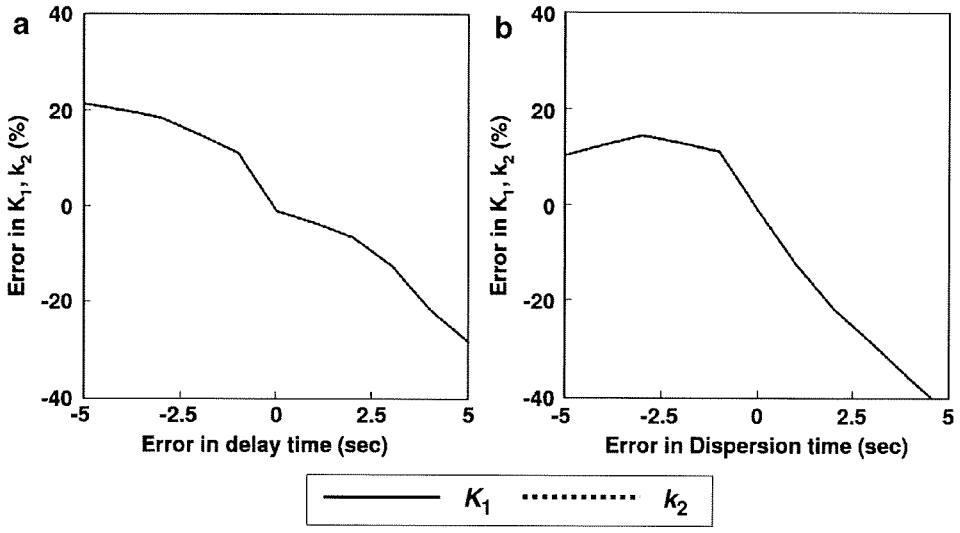

Fig. 5 Error propagation from the error in input time (**a**) and dispersion time constant (**b**) to K_1 and k_2 (the two lines were identical). Positive and negative values of error indicate over- and under-correction of delay time and dispersion time, respectively

estimate the rate constants of K_1 and/or k_2. Also V_A cannot be ignored, even when only relative rate constant values are needed. These findings suggest that the present k_2 obtained BFM technique provides an RBF image with reasonable accuracy and quality.

In the present study the rate constants of K_1 and k_2 were experimentally computed, and the ratios obtained ranged from 0.35 to 0.45 ml/g, which corresponds to the apparent kidney–blood partition coefficient. The much smaller apparent p value might be due to a partial volume effect, as has been demonstrated in a previous brain and cardiac study [10, 11], because of the composite structure of the kidney, the spatial resolution of the reconstructed image and breathing movement of the patient during the scan. When the rate constant K_1 is underestimated due to the partial volume effect, $k_2 \cdot p_{phys}$ could be applied for RBF rather than K_1. The present study showed that the contribution of GFR to the clearance rate was only 10%, and that $k_2 \cdot p_{phys}$ is more appropriate for RBF assessment, although further study of how the GFR changes under stimulated conditions is required. The $k_2 \cdot p_{phys}$ value in the cortical region obtained in the present study was 3.64±2.15 ml/min/g under normal condition, a value within the normal range of 4 to 5 ml/min/g reported in the literature [22]. Middlekauff et al. [23–25] applied the ROI base analysis, and showed similar RBF values around 4 ml/min/g. These findings also support the use of $k_2 \cdot p_{phys}$ for the calculation of RBF. The different values of RBF between the present study and the previous studies [3–5] might be due to differences in the approaches.

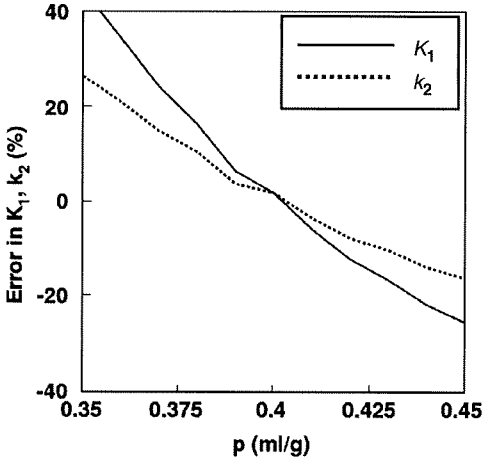

Fig. 6 Error propagation from the partition coefficient (p, ml/g) to K_1 and k_2. When the true p was varied between 0.6 and 0.8 ml/g, the size of the error in RBF was simulated assuming p=0.7 ml/g

The present computation of RBF by the BFM has two main advantages over the NLF. One is the ability to produce a voxel-by-voxel quantitative parametric map, and the other is faster computing speed. In fact, the parametric images were obtained within a reasonable time, i.e. 2.5 min with an image size of 128×128 pixels with 35 slices and 22 frames. The time could be further reduced by applying a threshold to omit pixels with lower values. From a clinical standpoint, voxel-by-voxel analysis is preferred to ROI-based analysis because the operator can independently define ROIs to improve reproducibility, and faster computations are important for analysing very large datasets.

Kinetic parameters estimated by the NLF agreed well with those estimated by the BFM as shown in Fig. 2. The disagreement in some rate constant values between the voxel-based (BFM) and ROI-based computation methods might have been due to the composite structure between the cortical region and its surroundings, or to image noise. Although superior to the NLF in terms of computing speed and ability to generate parametric maps, the BFM shares the same source of errors as the NLF because they use the

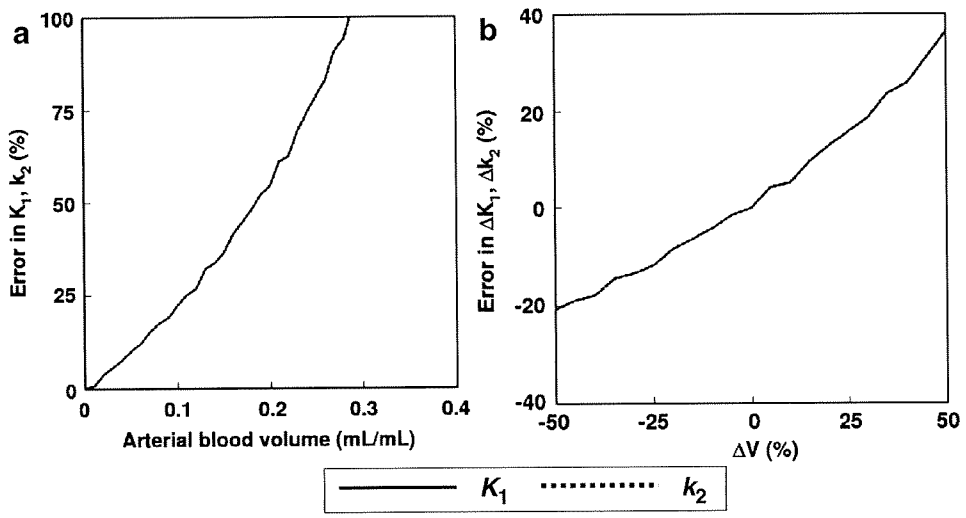

Fig. 7 **a** Error propagation from the arterial blood volume (V_A, ml/ml) to K_1 and k_2 (the two lines were identical). When the true V_A changed from 0.0 to 0.4 ml/ml, the size of the error in K_1 and k_2 calculated assuming V_A=0.0 ml/ml was simulated. **b** Error propagation from the change in arterial blood volume from 0.14 ml/ml (ΔV_A) to the change in K_1 and k_2 from the initial conditions (ΔK_1 and Δk_2, ml/min/g) (the two lines were identical)

same model and assumption. Delay and dispersion in input function, motion of the patient during a study [26–28], and flow heterogeneity [29] are sources of error for parameters estimated by both the NLF and BFM. Selection of a specific range of k_2 and the number of basis function can affect the accuracy and precision of the estimated parameters in neuroreceptor studies [30, 31]. However, the range was 0 to 15 ml/min/g in the present computation with $H_2{}^{15}O$, and the limits of this range would be acceptable for the present computation. In practice, selection of a wider range and/or a large number of discrete values of the basis function is slow and inefficient against the required accuracy and precision.

The present simulation study showed that if V_A is neglected or fixed, not only the absolute rate constants, i. e. RBF value, are overestimated, but estimated changes in RBF between two physiological states could be over- or underestimated. These findings suggest that V_A should be included to obtain either absolute or relative values of RBF. For p, the present simulation revealed that the error sensitivity in RBF for that value was significant. The values of p for the whole and cortical regions were 0.35 and 0.42 ml/g, respectively. If the value was fixed at 0.4 ml/g, a 40% overestimation in RBF for regions with a p of 0.35 occurred. Thus, regional difference in p introduce error in quantitative RBF values. Also the AIC analysis showed that introducing the extra parameters of p and V_A did not increase the AIC value against the others. These findings suggest that both p and V_A need to be estimated simultaneously with quantitative RBF, especially when changes under different conditions are assessed.

Knowledge of RBF is mostly needed in determining the severity of renovascular disease. Although the degree of renal artery stenosis is easily diagnosed, its actual effect on RBF remains difficult to quantify. In clinical work, estimates of GFR have not shown very good accuracy in relation to possible interventional treatment. Also, there is no good clinical method to easily measure single-kidney or regional RBF. We can obtain the effective renal plasma flow (ERPF) by infusing p-aminohippuric acid and measuring the urine and plasma concentrations, but this method only gives the total ERPF for both kidneys. An alternative is a magnetic resonance (MR) based method, which is problematic in patients with chronic kidney disease, because the contrast agent gadolinium is contraindicated in these subjects [32]. The present PET-related methodology may provide quantitative estimate of regional RBF, and be clinically applicable under conditions such as chronic allograft nephropathy and acute kidney insufficiency. The procedure – as presented here – still involves a small degree of invasiveness because of blood sampling. However, many noninvasive methods for estimating input functions have been proposed [3–5, 23–25, 33, 34], and their implementation will allow RBF to be determined in a fully noninvasive fashion, particularly for clinical purposes.

In conclusion, although some issues remain to be investigated, this study shows the feasibility of measurement of RBF using PET with $H_2{}^{15}O$.

Acknowledgments The authors thank the technical staff of the Turku PET Centre for their effort and skill dedicated to this project. This work was supported by the Hospital District of Southwest of Finland and was conducted within the "Centre of Excellence in Molecular Imaging in Cardiovascular and Metabolic Research" supported by the Academy of Finland, University of Turku, Turku University Hospital and Abo Academy. The study was further supported by grants from the Academy of Finland (206359 to P.N.), the Finnish Diabetes Foundation (P.I.), EFSD/Eli-Lilly (P.I.), the Sigrid Juselius Foundation (N.K. and P.I.), and the Novo Nordisk Foundation (P.N.).

References

1. Nitzsche EU, Choi Y, Killion D, Hoh CK, Hawkins RA, Rosenthal JT, et al. Quantification and parametric imaging of renal cortical blood flow in vivo based on Patlak graphical analysis. Kidney Int 1993;44:985–96.
2. Szabo Z, Xia J, Mathews WB, Brown PR. Future direction of renal positron emission tomography. Semin Nucl Med 2006;36:36–50.
3. Juillard L, Janier MF, Foucue D, Lionnet M, Le Bars D, Cinotti L, et al. Renal blood flow measurement by positron emission tomography using 15O-labeled water. Kidney Int 2000;57:2511–18.
4. Juillard L, Janier MF, Fouque D, Cinotti L, Maakel N, Le Bars D, et al. Dynamic renal blood flow measurement by positron emission tomography in patients with CRF. Am J Kidney Dis 2002;40:947–54.
5. Alpert NM, Rabito CA, Correia DJA, Babich JW, Littman BH, Tompkins RG, et al. Mapping of local renal blood flow with PET and H215O. J Nucl Med 2002;43:470–75.
6. Anderson HL, Yap JT, Miller MP, Robbins A, Jones T, Price PM. Assessment of pharmacodynamic vascular response in a phase I trial of combretastatin A4 phosphate. J Clin Oncol 2003;21:2823–30.
7. Anderson H, Yap JT, Wells P, Miller MP, Propper D, Price D, et al. Measurement of renal tumour and normal tissue perfusion using positron emission tomography in a phase II clinical trial of razoxane. Br J Cancer 2003;89:262–67.
8. Snyder WS, Cook MJ, Nasset ES, Karhausen LR, Howells GP, Tipton IH. Report of the Task Group on Reference Man. London: Pergamon Press; 1974. p. 175–77.
9. Herscovitch P, Raichle ME. What is the correct value for the brain–blood partition coefficient for water? J Cereb Blood Flow Metab 1985;5:65–9.
10. Iida H, Law I, Pakkenberg B, Krarup-Hansen A, Eberl S, Holm S, et al. Quantitation of regional cerebral blood flow corrected for partial volume effect using O-15 water and PET: I. Theory, error analysis, and stereologic comparison. J Cereb Blood Flow Metab 2000;20:1237–51.
11. Blomqvist G, Lammertsma AA, Mazoyer B, Wienhard K. Effect of tissue heterogeneity on quantification in positron emission tomography. Eur J Nucl Med 1995;22:652–63.
12. Koeppe RA, Holden JE, Ip WR. Performance comparison of parameter estimation techniques for the quantitation of local cerebral blood flow by dynamic positron computed tomography. J Cereb Blood Flow Metab 1985;5:224–34.
13. Gunn RN, Lammertsma AA, Hume SP, Cunningham VJ. Parametric imaging of ligand-receptor binding in PET using a simplified reference region model. Neuroimage 1997;6:279–87.
14. Watabe H, Jino H, Kawachi N, Teramoto N, Hayashi T, Ohta Y, et al. Parametric imaging of myocardial blood flow with 15O-water and PET using the basis function method. J Nucl Med 2005;46:1219–24.
15. Boellaard R, Knaapen P, Rijbroek A, Luurtsema GJ, Lammertsma AA. Evaluation of basis function and linear least squares methods for generating parametric blood flow images using 15O-water and positron emission tomography. Mol Imaging Biol 2005;7:273–85.
16. Ruotsalainen U, Raitakari M, Nuutila P, Oikonen V, Sipilä H, Teräs M, et al. Quantitative blood flow measurement of skeletal muscle using oxygen-15-water and PET. J Nucl Med 1997;38:314–19.
17. Levey A, Bosch J, Lewis J, Greene T, Rogers N, Roth D. A more accurate method to estimate glomerular filtration rate from serum creatinine: a new prediction equation. Modification of Diet in Renal Disease Study Group. Ann Intern Med 1999;130:461–70.
18. Iida H, Kanno I, Miura S, Murakami M, Takahashi K, Uemura K. Error analysis of a quantitative cerebral blood flow measurement using H215O autoradiography and positron emission tomography, with respect to the dispersion of the input function. J Cereb Blood Flow Metab 1986;6:536–45.
19. Iida H, Higano S, Tomura N, Shishido F, Kanno I, Miura S, et al. Evaluation of regional differences of tracer appearance time in cerebral tissues using [15O] water and dynamic positron emission tomography. J Cereb Blood Flow Metab 1988;8:285–88.
20. Akaike H. A new look at the statistical model identification. IEEE Trans Automat Contr 1974;AC19:716–23.
21. Kudomi N, Hayashi T, Teramoto N, Watabe H, Kawachi N, Ohta Y, et al. Rapid quantitative measurement of CMRO2 and CBF by dual administration of 15O-labeled oxygen and water during a single PET scan – a validation study and error analysis in anesthetized monkeys. J Cereb Blood Flow Metab 2005;259:1209–24.
22. Ganong WF. Review of medical physiology. 8th ed. Norwalk: Appleton & Lange; 1977. p. 522–45.
23. Middlekauff HR, Nitzsche EU, Hamilton MA, Schelbert HR, Fonarow GC, Moriguchi JD, et al. Evidence for preserved cardiopulmonary baroflex control of renal cortical blood flow in humans with advanced heart failure. Circulation 1995;92:395–401.
24. Middlekauff HR, Nitzsche EU, Hoh CK, Hamilton MA, Fonarow GC, Hage A, et al. Exaggerated renal vasoconstriction during exercise in heart failure patients. Circulation 2000;101:784–89.
25. Middlekauff HR, Nitzsche EU, Hoh CK, Hamilton MA, Fonarow GC, Hage A, et al. Exaggerated muscle mechanoreflex control of reflex renal vasoconstriction in heart failure. J Appl Physiol 2001;90:1714–19.
26. Fulton RR, Meikle SR, Eberl S, Pfeiffer J, Constable CJ. Correction for head movements in positron emission tomography using an optical motion-tracking system. IEEE Trans Nucl Sci 2002;49:116–23.
27. Bloomfield PM, Spinks TJ, Reed J, Schnorr L, Westrip AM, Livieratos L, et al. The design and implementation of a motion correction scheme for neurological PET. Phys Med Biol 2003;48:959–78.
28. Woo SK, Watabe H, Choi Y, Kim KM, Park CC, Iida H. Sinogram-based motion correction of PET images using optical motion tracking system and list-mode data acquisition. IEEE Trans Nucl Sci 2004;51:782–88.
29. Herrero P, Staudenherz A, Walsh JF, Gropler RJ, Bergmann SR. Heterogeneity of myocardial perfusion provides the physiological basis of perfusable tissue index. J Nucl Med 1995;36:320–27.
30. Cselényi Z, Olsson H, Halldin C, Gulyás B, Farde L. A comparison of recent parametric neuroreceptor mapping approaches based on measurements with the high affinity PET radioligands [11C]FLB 457 and [11C]WAY 100635. Neuroimage 2006;32:1690–708.
31. Schuitemaker A, van Berckel BN, Kropholler MA, Kloet RW, Jonker C, Scheltens P, et al. Evaluation of methods for generating parametric (R-[11C]PK11195 binding images. J Cereb Blood Flow Metab 2007;27:1603–15.
32. Martin D, Sharma P, Salman K, Jones RA, Grattan-Smith JD, Mao H, et al. Individual kidney blood flow measured with contrast-enhanced first-pass perfusion MR imaging. Radiology 2008;246:241–48.
33. Iida H, Kanno I, Takahashi A, Miura S, Murakami M, Takahashi K, et al. Measurement of absolute myocardial blood flow with H215O and dynamic positron-emission tomography strategy for quantification in relation to the partial-volume effect. Circulation 1988;78:104–15.
34. Germano G, Chen BC, Huang S-C, Gambhir SS, Hoffman EJ, Phelps ME. Use of the abdominal aorta for arterial input function determination in the hepatic and renal PET studies. J Nucl Med 1992;33:613–20.

Eur J Nucl Med Mol Imaging (2009) 36:1338–1345
DOI 10.1007/s00259-009-1094-0

ORIGINAL ARTICLE

Non-invasive diagnosis of acute mesenteric ischaemia using PET

Jan Kiss · Alexandru Naum · Nobuyuki Kudomi · Juhani Knuuti · Patricia Iozzo · Timo Savunen · Pirjo Nuutila

Received: 14 December 2008 / Accepted: 4 February 2009 / Published online: 11 March 2009

Abstract
Purpose Acute mesenteric ischaemia (AMI) is a lethal disease with an increasing incidence. Despite the availability of effective treatment, AMI remains a vascular emergency with over 60% mortality rate mainly due to late diagnosis. The difficulty in diagnosing this fatal condition stems from non-specific clinical and laboratory findings and lack of appropriate imaging study. Our aim was to test a non-invasive method of identifying AMI using PET.
Methods The study was conducted in normal pigs (n=14), sham-operated pigs (n=4) and pigs undergoing ischaemia and reperfusion of intestine (n=6). Liver blood flow was imaged by $H_2{}^{15}O$ PET and liver blood content by $C^{15}O$ PET. Both scans were performed during intestinal ischaemia and during reperfusion.
Results AMI was identified by PET imaging of hepatic perfusion and blood pool. The $H_2{}^{15}O$ PET scan during AMI detected a 40% decrease in total liver perfusion, which was caused by a 45% reduction of portal blood flow and no alteration in arterial blood flow. Compromised hepatic perfusion during AMI was accompanied by a 75% decrease in hepatic blood pool recognized by the $C^{15}O$ PET scan. The striking reduction of liver blood flow and blood content persisted during reperfusion of intestine.
Conclusion Our results demonstrate that AMI can be readily recognized by PET imaging of liver blood flow and blood content. Moreover, PET can be used in detection of perfusion abnormalities after revascularization. This non-invasive imaging tool could represent a novel approach to diagnose AMI.

Keywords Acute mesenteric ischaemia · Intestinal ischaemia · Positron emission tomography · PET

J. Kiss · A. Naum · N. Kudomi · J. Knuuti · P. Iozzo · P. Nuutila
Turku PET Center, Centre of Excellence in Molecular Imaging in Cardiovascular and Metabolic Research supported by the Academy of Finland, University of Turku, Turku University Hospital and Abo Academy, P.O. Box 52, 20521 Turku, Finland

J. Kiss · T. Savunen
Department of Surgery, Turku University Central Hospital, P.O. Box 52, 20521 Turku, Finland

P. Iozzo
Institute of Clinical Physiology, National Research Council (CNR), Via Moruzzi 1 56124 Pisa, Italy

J. Kiss (✉)
Department of Cardiovascular Surgery, University Medical Center Freiburg, Hugstetterstrasse 55, 79106 Freiburg, Germany
e-mail: jan.kiss@uniklinik-freiburg.de

Introduction

Acute mesenteric ischaemia (AMI) represents one of the most dramatic vascular emergencies. This condition is characterized by a sudden occlusion of mesenteric arteries followed by impairment of intestinal blood flow [1]. The occlusion is most frequently caused by embolism or arterial thrombosis. Emboli originate from the heart or from a proximal artery and thrombosis is usually a consequence of atherosclerosis or arterial dissection. The incidence of AMI has been increasing due to longer mean life expectancy [2]. Despite the progress in surgical and intensive care during recent decades, the reported mortality rates remain over 60% [3–6]. The major reason behind extremely high mortality is the difficulty in recognizing

this condition. A recent study showed that most of the patients are treated more than 24 h after the onset of the symptoms [7]. Non-specific clinical and laboratory findings delay diagnosis of AMI. Non-invasive imaging studies at the early stage of the disease are associated with low sensitivity and specificity. These imaging techniques can reliably diagnose AMI at the late stage of the disease, when necrosis of the intestine has already developed. At that point, the spillover of bacteria and endotoxin from the necrotic intestine to the circulation triggers systemic inflammation, multiple organ failure and death [1]. Therefore, early diagnosis and treatment of AMI are the key factors that can reduce the high mortality rate.

Diagnosis of AMI could be accelerated by appropriate imaging studies. The lack of consensus on which imaging modality should be used results in late application of diagnostic tools [8–10]. Plain X-ray and computed tomography (CT) detect in most cases late findings, such as pneumatosis intestinalis, portal venous gas or signs of intestinal perforation [11–14]. CT angiography was shown to be insufficiently sensitive, unless the above-mentioned late findings are taken into account [15]. Low resolution of magnetic resonance imaging (MRI) might not be sufficient to detect occlusion of smaller intestinal vessels [16, 17]. Duplex ultrasonography of deeply located mesenteric arteries can detect their obstruction only in a patient without excessive intestinal gas. Due to the poor imaging conditions in an emergency setting duplex scanning as a diagnostic method for AMI detection is contraindicated [18, 19]. The use of arteriography is similarly controversial because of its invasiveness and time requirement [19, 20]. Thus, there is obvious need for a new non-invasive technique capable of imaging of splanchnic circulation.

Results from experimental studies using invasive measurements showed that AMI causes a dramatic decrease in liver blood flow [21–23]. Reduction of portal blood flow is associated with a decrease of portal pressure and results in a decrease of the hepatic blood volume [24]. Both hepatic blood flow and blood content can be measured non-invasively by PET [25, 26]. PET imaging of liver circulation could therefore be a novel method for diagnosis of AMI. In addition, PET could be used to recognize persisting deficits in liver circulation after revascularization of intestine.

The aim of the present study was to test whether established methods of measuring hepatic perfusion and blood content by PET are capable of detecting AMI. To assess the impact of intestinal reperfusion on liver circulation, the same parameters were measured after re-establishing blood flow to the intestine. The study was conducted in pigs in order to standardize the conditions in all of the groups.

Materials and methods

Animal instrumentation

Twenty-four weight-matched pigs were used in the experiments (30.2±0.7 kg). The animals were deprived of food 12 h before the experiment. Water was withheld only 1 h prior to surgery. Details of the procedure were reported previously [26]. Briefly, the animals were premedicated with ketamine (34 mg/kg i.m.) and diazepam (10 mg i.v.). After administration of pancuronium (4 mg i.v.), the animals were intubated via tracheotomy. The animals were connected to a volume-triggered respirator and ventilated with room air at the frequency of 16 breaths/min. The anaesthesia was maintained with continuous intravenous infusion of ketamine (0.27 mg/kg per min) and pancuronium (0.007 mg/kg per min). The internal carotid artery, external jugular vein, portal vein and hepatic vein were cannulated for blood sampling and the femoral vein for administration of tracers. The animals were divided into three groups: (1) healthy (n=14), which were left unchallenged (data previously published for validation purposes [25, 26]), (2) sham (n=4), which underwent sham operation identical with the procedure performed in the AMI group except for induction of intestinal ischaemia and (3) AMI (n=6), which underwent intestinal ischaemia induced by clamping of the superior mesenteric artery (SMA) for 60 min. Vital signs, blood pressure and heart rate were monitored throughout the study.

The study protocol was reviewed and approved by the Ethics Committee for Animal Experiments of the University of Turku.

PET scanning

PET acquisition was carried out in 2-D mode using an ECAT 931-08/12 scanner (CTI Inc, Knoxville, TN, USA) with a 10.5-cm axial field of view and a resolution of 6.7 mm (axial)×6.5 mm (in-plane) full-width at half-maximum. The scheme of the study design is shown in Fig. 1.

After acquisition of a transmission scan to correct for photon attenuation, animals were administered $C^{15}O$ by inhalation. Hepatic blood pool was imaged by a static scan.

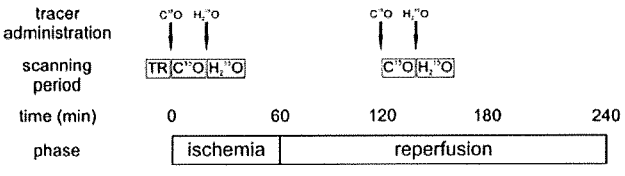

Fig. 1 Study design. The *arrows* indicate tracer administration, the *white boxes* represent scanning periods and the *grey boxes* the phase of the disease. TR – transmission

Radioactivity concentration during the imaging period was measured from three arterial blood samples obtained at equilibrium. Shortly after completing the $C^{15}O$ scan, $H_2{}^{15}O$ was administered by intravenous injection. Data were collected over a period of 6 min in 6×5, 6×15 and 8×30 s frames. Both scans were repeated 120 min later.

Image processing

Dynamic sinogram data were corrected for dead time in each frame in addition to detector normalization. Tomographic images were reconstructed from corrected sinogram data by the median root prior reconstruction algorithm with 150 iterations and Bayesian coefficient of 0.3 [27]. Attenuation correction was applied with transmission data. A reconstructed image had 128×128×15 matrix size with a pixel size of 2.4 mm×2.4 mm and 6.7 mm with 20 frames.

Data processing

Liver blood content was calculated as described previously [26]. For production of ^{15}O compounds, a low-energy deuteron accelerator, Cyclone 3 was used (Ion Beam Application, Louvain-la-Neuve, Belgium). [^{15}O]-oxygen is processed to [^{15}O]CO in a charcoal oven at 950°C. Before each study, gas chromatographic analysis was performed to verify the purity of the product. Production of 5 GBq/min for [^{15}O]-oxygen and 3 GBq/min for [^{15}O]CO was achieved with a nominal 50 kA target current when the gas flow was 0.5 L/min. The administered activities were monitored, and the inhaled radioactive dose was measured using a low-voltage ionization chamber.

For measurement of liver blood volume each subject inhaled [^{15}O]CO for 2 minutes through a three-way inhalation flap-valve (0.14% CO mixed with room air). The exhaled radioactivity was disposed to waste. After the 2 minutes inhalation time, another 2 minutes were allowed for CO to combine with haemoglobin before a static scan was started for 4 minutes. During the scan period, three blood samples were drawn at 4, 6, and 8 min from the beginning of the inhalation, and their radioactivity concentration was measured with an automatic gamma counter (1480 Wizard, Wallac, Turku). An additional blood sample was drawn and spun, and the plasma radioactivity concentration was measured to verify that all [^{15}O]CO was bound to red blood cells and was not transformed into carbon dioxide in the plasma. Plasma radioactivity was always < 1% of that in the blood.

A region of interest (ROI) was drawn in the liver in four representative transaxial slices in each study. Values of blood volume were calculated according to a previously published method [28]. The blood volume in liver tissue was determined by dividing the tissue radioactivity concentration by concentration in blood, according to the following formula:

$$V_B = \frac{C_{PET}}{C_{BLOOD} \times \rho_{liver\ tissue} \times 0.85} \times 100, \text{ where}$$

V_B is the blood volume of a liver region (in ml blood/ 100 g liver tissue), C_{PET} is the activity in the liver ROI (in Bq/ml liver), C_{BLOOD} is the activity in the blood (in Bq/ml blood), $\rho_{liver\ tissue}$ is liver tissue density (in g/ml) and 0.85 represent the tissue-to-large vessel haematocrit ratio. Specific density of liver (1.04 g/ml) was taken into account to express the blood volume results as milliliters per 100 g of liver.

Hepatic artery and portal vein flows were measured using a previously published method [25]. [^{15}O]H_2O was produced as previously described by dialysis technique in a continuously working water module [29, 30]. Briefly, [^{15}O]H_2O was produced by reaction of N_2 + 2% $^{15}O_2$ mixture and H_2 over a heated palladium catalyst to form [^{15}O]H_2O, which was mixed with physiological saline solution. Sterility and pyrogenicity tests for water were performed to verify the purity of the product.

[^{15}O]H_2O was injected intravenously for 2 min using an automated infusion pump with an infusion rate of 240 ml/h. Data were collected over a period of 6 min in 6×5, 6×15 and 8×30 s frames.

The input function was estimated and obtained from dynamic liver images. The method introduces a model function in a form as:

$$\begin{aligned} C_{\mathrm{AIF}}(t) &= 0. && (t < t_1) \\ &= A\frac{1-\exp\left(K_e(1+\alpha)(t_1-t)\right)}{1+\alpha} && (t_1 < t < t_2) \\ &= A\frac{\exp\left(K_e(1+\alpha)(t_1-t_2)\right)+\exp\left(K_e(1+\alpha)(t_2-t)\right)-2\cdot\exp\left(K_e(1+\alpha)(t_1-t)\right)}{1+\alpha} && (t > t_2) \end{aligned}$$

In this formula, the tracer is assumed to be administrated as a rectangular shape, where t_1 and t_2 indicate the start and end time of tracer administration in addition to the transit time from administration location to liver region; A is height. After the administration, it is assumed that the tracer diffuses between arterial blood to whole-body interstitial

spaces with rates K_e (ml/min) and K_i (ml/min), respectively; α was defined as: K_i/K_e. $C_{WB}(t)$ assumes the tracer concentration in whole-body peripheral tissue. Portal vein blood TAC was generated by assuming a gut compartment model with diffusion rate k_g [31, 32] as:

$$C_P = k_g C_A(t+\Delta t) \otimes e^{-k_g \cdot (t+\Delta t)}$$

Using those model functions, the time activity curve for the hepatic region measured by PET (C_L Bq/ml) can be expressed, including the blood volume term (V_0 ml/ml) as:

$$C_L(t) = (1-V_0)\left(f_a C_A(t) + f_p C_p(t)\right) \otimes e^{-k_2 \cdot t} + V_0\left(f_a C_A(t) + f_p C_p(t)\right) / \left(f_a + f_p\right)$$

where f_a (ml/min per g) and f_p (ml/min per g) are arterial and portal vein blood flow, respectively, and k_2 is defined as $(f_a+f_p)/V_L$, V_L (g/ml), fixed to 0.7 g/ml in the present input estimation [33], is a distribution volume of water between blood and tissue.

An ROI was placed on the whole region of the liver in a summed image that was divided into clusters slice by slice so that the size of each cluster consisted of 120 pixels. Tissue time activity curves in those clusters were extracted from the dynamic image. Then, input function was estimated as follows: first, the model function in the equation was fitted to each extracted tissue curve individually and a set of six parameters of A, t_1, t_2, K_e, α and r ($=f_a/f_p$) was obtained for each tissue TAC. In the second step, fixing values of parameters of t_1, t_2, α and r as their means, the other two parameters of A and K_e were estimated by the grid search method by minimizing the following equation:

$$S^2 = \sum_{i \in Tis} \sum_{k} \left(C_L^{i,k} - \left(\begin{array}{l} (1-V_0^i)\left(f_a^i C_A(t) + f_p^i C_p(t)\right) \otimes e^{-k_2^i \cdot t} \\ + V_0^i \frac{f_a^i C_A(t) + f_p^i C_p(t)}{f_a^i + f_p^i} \end{array} \right) \right)^2$$

where $C_L^{i,k}$ is the activity concentration for kth frame in ith cluster, t is the corresponding time of kth frame, and f_a^i, f_v^i and V_0^i are values of arterial and portal vein blood flows, and blood volume for ith tissue, respectively.

Flow values of f_a, f_p and V_0 were calculated by the non-linear fitting method (Gauss-Newton method) from the input function estimated from the tissue curve for the whole liver region.

Total hepatic blood flow was calculated as the sum of arterial hepatic blood flow and portal hepatic blood flow. This technique enables a quantitative estimation of liver perfusion through both vessels from $H_2{}^{15}O$ PET images with a completely non-invasive approach.

Statistical analysis

All data are shown as mean±SEM. Non-parametric one-way ANOVA (Kruskal-Wallis and Mann-Whitney U tests) and repeated measures ANOVA were used where appropriate; $p<0.05$ was considered statistically significant.

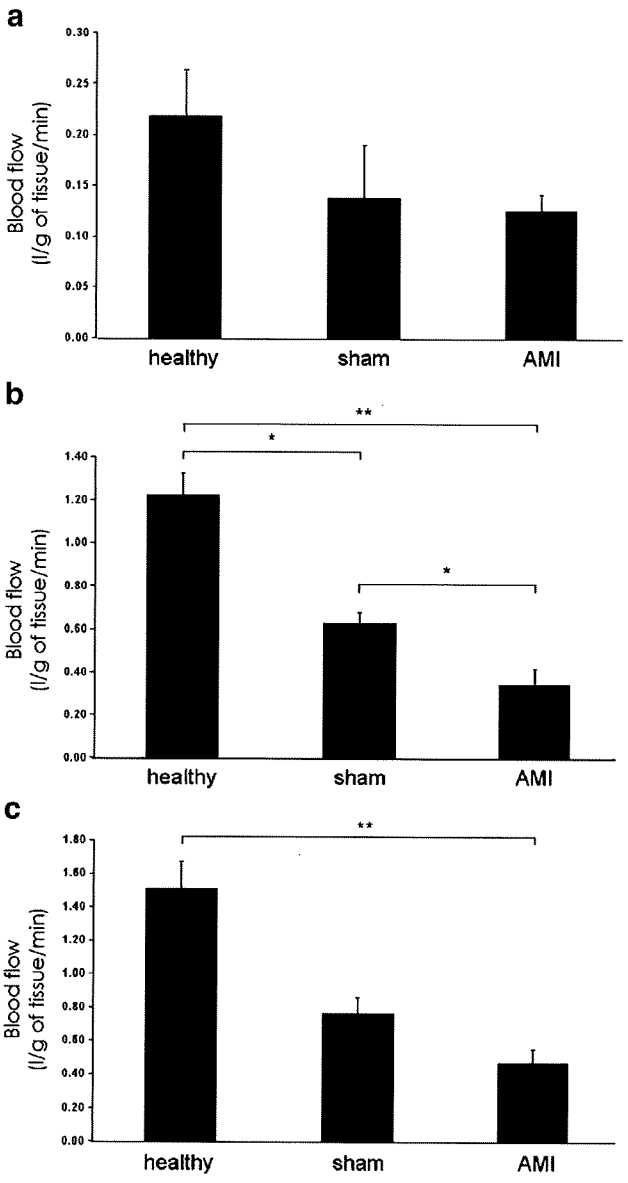

Fig. 2 Intestinal ischaemia is detected by measurement of liver perfusion using PET. Animals were left unchallenged (healthy, $n=14$), underwent sham operation (sham, $n=4$) or induction of intestinal ischaemia (AMI, $n=6$). Arterial (**a**), portal (**b**) and total liver blood flow (**c**) during ischaemia were measured by PET after injection of $H_2{}^{15}O$ (mean±SEM). *$p<0.05$; **$p<0.01$

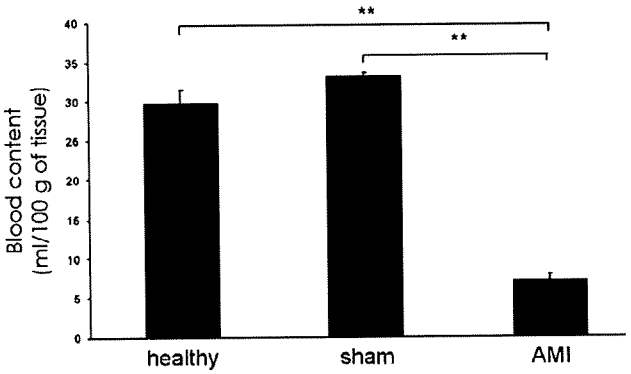

Fig. 3 Intestinal ischaemia results in reduction of liver blood content. Hepatic blood content during ischaemia was measured by PET after inhalation of $C^{15}O$ in healthy, sham-operated and ischaemic pigs (mean±SEM). *$p<0.05$; **$p<0.01$

Results

Liver perfusion using PET

The $H_2{}^{15}O$ PET scan revealed profound changes in hepatic perfusion during AMI (Fig. 2). Total liver blood flow was decreased by 39% when compared to sham-operated animals ($p=0.06$) and by 69% when compared to the healthy controls ($p=0.0007$). Liver perfusion from the portal vein was reduced by 45% in comparison to the sham-operated animals ($p=0.04$) and by 72% in comparison to the healthy controls ($p=0.0001$). On the contrary, there were no significant changes in the liver perfusion via the hepatic artery.

PET imaging of liver blood content

Using the $C^{15}O$ PET scan, we identified a striking decrease in hepatic blood content during AMI (Fig. 3). We observed a 75% ($p=0.001$) and a 76% ($p=0.000002$) decrease in liver blood content during intestinal ischaemia when compared to the sham-operated animals and healthy controls, respectively. We conclude that a decrease in liver blood flow is accompanied by a decrease in blood content.

Hepatic perfusion and liver blood content after re-establishment of intestinal blood flow

The no-reflow phenomenon is a known component of the reperfusion syndrome [34]. We found that hypoperfusion of the liver persisted also after reperfusion of the intestine (Fig. 4). In our model, total liver blood flow was decreased by 27% ($p=0.004$) when compared to sham-operated animals. The portal vein component of liver blood flow was reduced by 32% in comparison to the sham-operated

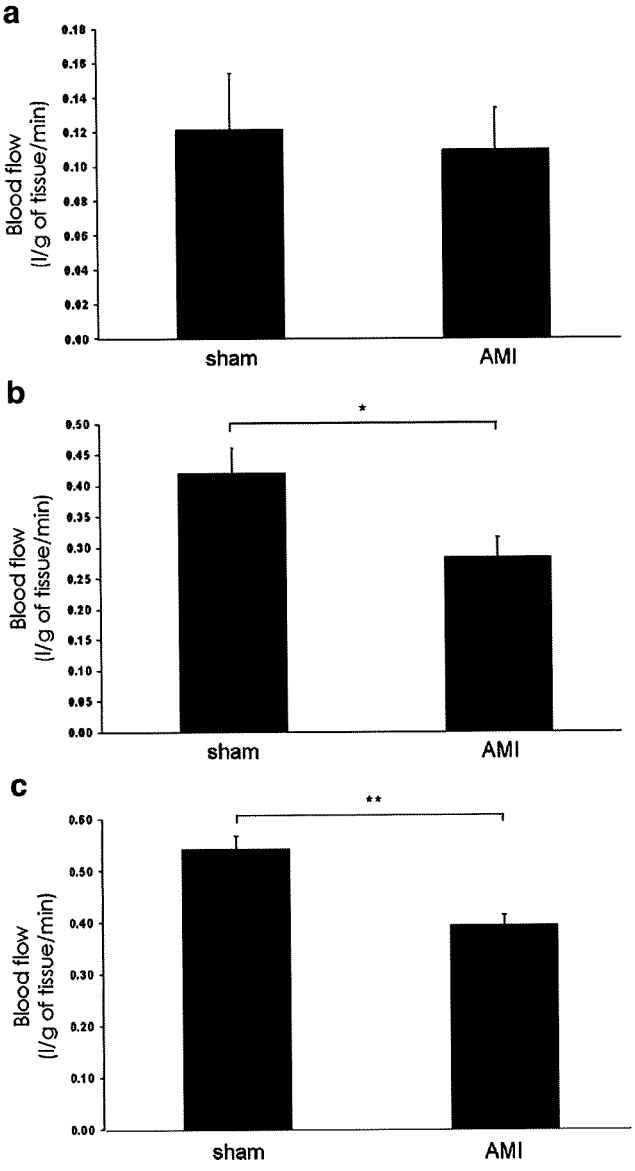

Fig. 4 Hepatic perfusion remains compromised despite re-establishment of intestinal blood flow. Pigs underwent sham operation or intestinal ischaemia followed by reperfusion. Arterial (**a**), portal (**b**) and total liver blood flow (**c**) during reperfusion were measured by PET after injection of $H_2{}^{15}O$ (mean±SEM). *$p<0.05$; **$p<0.01$

animals ($p=0.04$). Similarly to ischaemia, there were no significant changes in the liver perfusion via the hepatic artery during reperfusion.

We detected a severe decrease in hepatic blood content after reperfusion of intestine (Fig. 5). Liver blood content was reduced by 64% ($p=0.04$) in comparison to the sham-operated animals after intestinal ischaemia and reperfusion. Therefore, our data indicate that a decrease in liver blood flow is associated with a decrease in liver blood content.

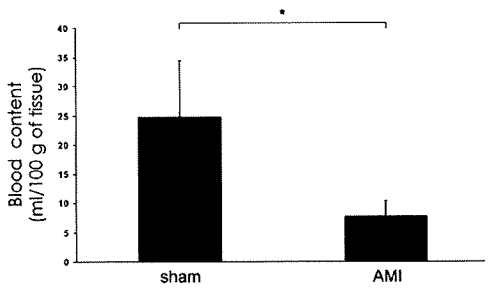

Fig. 5 Severe reduction of liver blood content persists during reperfusion of ischaemic intestine. Hepatic blood content during reperfusion was measured by PET after inhalation of $C^{15}O$ in sham-operated and ischaemic pigs (mean±SEM). *$p<0.05$; **$p<0.01$

Discussion

This is the first study to show that PET imaging of liver circulation can recognize AMI. Both liver blood flow and blood content are dramatically reduced during AMI. These parameters can be detected non-invasively by $H_2{}^{15}O$ and $C^{15}O$ PET. In addition, our data show that liver PET imaging is capable of identifying compromised liver circulation during reperfusion of ischaemic intestine. Hence, PET could be used both in the diagnosis of AMI and in the follow-up after revascularization.

AMI is a fatal disease caused by an insufficient blood flow to the intestine or its part. The most common causes of obstructive AMI are embolism or thrombosis of mesenteric arteries [8]. Mortality remains high mainly due to late diagnosis [7–10]. There are several imaging methods which in theory should be capable of diagnosing AMI, but each of them has certain drawbacks [7–10, 13, 14, 18, 20]. Therefore, there is need for a non-invasive imaging method capable of early diagnosis of AMI.

Intestinal ischaemia is associated with a decreased hepatic perfusion [21–23]. We observed an almost 40% reduction of total hepatic blood flow during intestinal ischaemia. This decrease was caused by a 45% decrease of portal hepatic perfusion. Liver blood flow from the hepatic artery remained unchanged. The sham-operated animals suffered from a certain degree of hepatic hypoperfusion when compared to the healthy controls due to more complex surgery. In earlier studies, the authors observed about a 40% reduction of total hepatic blood flow and a 40–65% reduction of portal blood flow [21–23]. Hence, it appears that non-invasive measurement by PET is capable of detecting changes of hepatic perfusion during intestinal ischaemia with similar accuracy as invasive blood flow measurement, which required surgical access to the portal vein and hepatic artery.

The liver receives blood supply via two routes: portal vein and hepatic artery (75 and 25% of hepatic blood flow, accordingly). In low flow states, such as cardiogenic shock or haemorrhage, a decrease in hepatic perfusion is caused by reduction of flow in both vessels. In contrast, AMI leads to reduction of portal flow only. Thus, the findings of the present study are in agreement with what can be expected from the pathophysiology. The clinical relevance of this phenomenon is that since the liver is so dependent on blood supply from the portal vein, it works as a great surrogate to assess disturbances in blood flow in the intestine and thus can be used as a diagnostic tool to detect intestinal ischaemia.

Hepatic blood flow was in the current study measured using estimated hepatic arterial and portal input functions from the PET image. This method was shown to be accurate and corresponds to the blood flow measured by ultrasonography, which is the gold standard for blood flow estimation [25]. The reproducibility of the non-invasive measurement of hepatic blood flow was tested by comparing two independent estimations in the same subject. The reproducibility was tested in four subjects. The difference between the two estimations was 3.5±13.5% and 2.6±6.2% for arterial and portal blood flow, respectively.

Our results and the earlier studies show that the liver suffers from hypoperfusion during intestinal ischaemia [21–23, 35]. Occlusion of the SMA results in a dramatic reduction of portal pressure and hepatic blood volume [35, 36]. Thus, the compliant vascular bed of the liver allows for adjustments of hepatic blood volume in response to liver blood flow [24]. In our model, a 40% decrease of hepatic perfusion resulted in a 75% reduction of liver blood content. This striking decrease of hepatic blood content is most likely caused by a combination of the passive collapse of capillaries and ischaemic changes, which further reduce the intravascular space in the liver [34].

Reperfusion worsens the microcirculatory dysfunction of the liver initiated by ischaemia. Vasoconstriction and capillary plugging interfere with reperfusion, prolonging ischaemia in the reperfused organ [34]. Horie et al. observed in mice an over 20% reduction in perfused sinusoids [37]. In our model, hepatic blood flow in pigs was reduced by almost 30%. More pronounced hepatic hypoperfusion can be explained by use of different animal species, different methods to estimate the blood flow and longer periods of ischaemia and reperfusion.

The methods used in this study have been previously shown to accurately quantitate the liver blood flow and blood content. Each of these methods readily detects AMI. The advantage of blood flow measurement is that this method gives information about liver perfusion through both the portal vein and hepatic artery. In contrast, hepatic blood content reflects a decreased portal flow but gives no information about hepatic arterial flow. Based on the current data both blood volume and portal blood flow seem to identify AMI, but further clinical studies are warranted to explore the clinical value of each parameter.

In conclusion, our data introduce liver PET imaging as a novel non-invasive diagnostic tool for detection of AMI. AMI is associated with a reduction of liver perfusion and blood content, which can be imaged by $H_2{}^{15}O$ and $C^{15}O$ PET, respectively. Moreover, we provide evidence that PET is a useful tool in detection of persisting disturbances of liver perfusion and blood content during reperfusion of the intestine. Clinical studies of liver PET imaging are warranted to ensure the performance of this technique in clinical setting in the patients suspected of having AMI.

References

1. Yasuhara H. Acute mesenteric ischemia: the challenge of gastroenterology. Surg Today 2005;35:185–95. doi:10.1007/s00595-004-2924-0.
2. Björck M, Troëng T, Bergqvist D. Risk factors for intestinal ischaemia after aortoiliac surgery: a combined cohort and case-control study of 2824 operations. Eur J Vasc Endovasc Surg 1997;13:531–9. doi:10.1016/S1078-5884(97)80061-5.
3. Andersson R, Pärsson H, Isaksson B, Norgren L. Acute intestinal ischemia. A 14-year retrospective investigation. Acta Chir Scand 1984;150:217–21.
4. Mamode N, Pickford I, Leiberman P. Failure to improve outcome in acute mesenteric ischaemia: seven-year review. Eur J Surg 1999;165:203–8.
5. Endean ED, Barnes SL, Kwolek CJ, Minion DJ, Schwarcz TH, Mentzer RM Jr. Surgical management of thrombotic acute intestinal ischemia. Ann Surg 2001;233:801–8. doi:10.1097/00000658-200106000-00010.
6. Dahlke MH, Asshoff L, Popp FC, Feuerbach S, Lang SA, Renner P, et al. Mesenteric ischemia—outcome after surgical therapy in 83 patients. Dig Surg 2008;25:213–9. doi:10.1159/000140692.
7. Kassahun WT, Schulz T, Richter O, Hauss J. Unchanged high mortality rates from acute occlusive intestinal ischemia: six year review. Langenbecks Arch Surg 2008;393:163–71. doi:10.1007/s00423-007-0263-5.
8. Schoots IG, Koffeman GI, Legemate DA, Levi M, van Gulik TM. Systematic review of survival after acute mesenteric ischaemia according to disease aetiology. Br J Surg 2004;91:17–27. doi:10.1002/bjs.4459.
9. Oldenburg WA, Lau LL, Rodenberg TJ, Edmonds HJ, Burger CD. Acute mesenteric ischemia: a clinical review. Arch Intern Med 2004;164:1054–62. doi:10.1001/archinte.164.10.1054.
10. Sreenarasimhaiah J. Diagnosis and management of intestinal ischaemic disorders. BMJ 2003;326:1372–6. doi:10.1136/bmj.326.7403.1372.
11. Wiesner W, Khurana B, Ji H, Ros PR. CT of acute bowel ischemia. Radiology 2003;226:635–50. doi:10.1148/radiol.2263011540.
12. Khurana B, Ledbetter S, McTavish J, Wiesner W, Ros PR. Bowel obstruction revealed by multidetector CT. AJR Am J Roentgenol 2002;178:1139–44.
13. Greenwald DA, Brandt LJ, Reinus JF. Ischemic bowel disease in the elderly. Gastroenterol Clin North Am 2001;30:445–73. doi:10.1016/S0889-8553(05)70190-4.
14. Smerud MJ, Johnson CD, Stephens DH. Diagnosis of bowel infarction: a comparison of plain films and CT scans in 23 cases. AJR Am J Roentgenol 1990;154:99–103.
15. Kirkpatrick ID, Kroeker MA, Greenberg HM. Biphasic CT with mesenteric CT angiography in the evaluation of acute mesenteric ischemia: initial experience. Radiology 2003;229:91–8. doi:10.1148/radiol.2291020991.
16. Laissy JP, Trillaud H, Douek P. MR angiography: noninvasive vascular imaging of the abdomen. Abdom Imaging 2002;27:488–506. doi:10.1007/s00261-001-0063-2.
17. Gilfeather M, Holland GA, Siegelman ES, Schnall MD, Axel L, Carpenter JP, et al. Gadolinium-enhanced ultrafast three-dimensional spoiled gradient-echo MR imaging of the abdominal aorta and visceral and iliac vessels. Radiographics 1997;17:423–32.
18. Hata J, Kamada T, Haruma K, Kusunoki H. Evaluation of bowel ischemia with contrast-enhanced US: initial experience. Radiology 2005;236:712–5. doi:10.1148/radiol.2362040299.
19. Hirsch AT, Haskal ZJ, Hertzer NR, Bakal CW, Creager MA, Halperin JL, et al. ACC/AHA 2005 Practice Guidelines for the management of patients with peripheral arterial disease (lower extremity, renal, mesenteric, and abdominal aortic): a collaborative report from the American Association for Vascular Surgery/Society for Vascular Surgery, Society for Cardiovascular Angiography and Interventions, Society for Vascular Medicine and Biology, Society of Interventional Radiology, and the ACC/AHA Task Force on Practice Guidelines (Writing Committee to Develop Guidelines for the Management of Patients With Peripheral Arterial Disease): endorsed by the American Association of Cardiovascular and Pulmonary Rehabilitation; National Heart, Lung, and Blood Institute; Society for Vascular Nursing; TransAtlantic Inter-Society Consensus; and Vascular Disease Foundation. Circulation 2006;113:e463–54. doi:10.1161/CIRCULATIONAHA.106.174526.
20. Lefkovitz Z, Cappell MS, Lookstein R, Mitty HA, Gerard PS. Radiologic diagnosis and treatment of gastrointestinal hemorrhage and ischemia. Med Clin North Am 2002;86:1357–99. doi:10.1016/S0025-7125(02)00080-9.
21. Bracht H, Takala J, Tenhunen JJ, Brander L, Knuesel R, Merasto-Minkkinen M, et al. Hepatosplanchnic blood flow control and oxygen extraction are modified by the underlying mechanism of impaired perfusion. Crit Care Med 2005;33:645–53. doi:10.1097/01.CCM.0000156445.59009.49.
22. Jakob SM, Tenhunen JJ, Heino A, Pradl R, Alhava E, Takala J. Splanchnic vasoregulation during mesenteric ischemia and reperfusion in pigs. Shock 2002;18:142–7. doi:10.1097/00024382-200208000-00009.
23. Jakob SM, Merasto-Minkkinen M, Tenhunen JJ, Heino A, Alhava E, Takala J. Prevention of systemic hyperlactatemia during splanchnic ischemia. Shock 2000;14:123–7. doi:10.1097/00024382-200014020-00008.
24. Lautt WW. Regulatory processes interacting to maintain hepatic blood flow constancy: vascular compliance, hepatic arterial buffer response, hepatorenal reflex, liver regeneration, escape from vasoconstriction. Hepatol Res 2007;37:891–903. doi:10.1111/j.1872-034X.2007.00148.x.
25. Kudomi N, Slimani L, Järvisalo MJ, Kiss J, Lautamäki R, Naum GA, et al. Non-invasive estimation of hepatic blood perfusion from H(2) (15)O PET images using tissue-derived arterial and portal input functions. Eur J Nucl Med Mol Imaging 2008;35:1899–911.
26. Iozzo P, Jarvisalo MJ, Kiss J, Borra R, Naum GA, Viljanen A, et al. Quantification of liver glucose metabolism by positron emission tomography: validation study in pigs. Gastroenterology 2007;132:531–42. doi:10.1053/j.gastro.2006.12.040.
27. Alenius S, Ruotsalainen U. Bayesian image reconstruction for emission tomography based on median root prior. Eur J Nucl Med 1997;24:258–65.
28. Grubb RL Jr, Raichle ME, Higgins CS, Eichling JO. Measurement of regional cerebral blood volume by emission tomography. Ann Neurol 1978;4:322–8. doi:10.1002/ana.410040407.

29. Clark JC, Crouzel C, Meyer GJ, Strijckmans K. Current methodology for oxygen-15 production for clinical use. Int J Rad Appl Instrum [A] 1987;38:597–600. doi:10.1016/0883-2889(87)90122-5.
30. Pinard E, Mazoyer B, Verrey B, Pappata S, Crouzel C. Rapid measurement of regional cerebral blood flow in the baboon using 15O-labelled water and dynamic positron emission tomography. Med Biol Eng Comput 1993;31:495–502. doi:10.1007/BF02441985.
31. Ziegler SI, Haberkorn U, Byrne H, Tong C, Kaja S, Richolt JA, et al. Measurement of liver blood flow using oxygen-15 labelled water and dynamic positron emission tomography: limitations of model description. Eur J Nucl Med 1996;23:169–77.
32. Taniguchi H, Yamaguchi A, Kunishima S, Koh T, Masuyama M, Koyama H, et al. Using the spleen for time-delay correction of the input function in measuring hepatic blood flow with oxygen-15 water by dynamic PET. Ann Nucl Med 1999;13:215–21.
33. Slimani L, Kudomi N, Oikonen V, Jarvisalo M, Kiss J, Naum A, et al. Quantification of liver perfusion with [(15)O]H(2)O-PET and its relationship with glucose metabolism and substrate levels. J Hepatol 2008;48:974–82.
34. Montalvo-Jave EE, Escalante-Tattersfield T, Ortega-Salgado JA, Piña E, Geller DA. Factors in the pathophysiology of the liver ischemia-reperfusion injury. J Surg Res 2008;147:153–9. doi:10.1016/j.jss.2007.06.015.
35. Groszmann RJ, Blei AT, Kniaz JL, Storer EH, Conn HO. Portal pressure reduction induced by partial mechanical obstruction of the superior mesenteric artery in the anesthetized dog. Gastroenterology 1978;75:187–92.
36. Lautt WW, Brown LC, Durham JS. Active and passive control of hepatic blood volume responses to hemorrhage at normal and raised hepatic venous pressure in cats. Can J Physiol Pharmacol 1980;58:1049–57.
37. Horie Y, Wolf R, Flores SC, McCord JM, Epstein CJ, Granger DN. Transgenic mice with increased copper/zinc-superoxide dismutase activity are resistant to hepatic leukostasis and capillary no-reflow after gut ischemia/reperfusion. Circ Res 1998;83:691–6.

Eur J Nucl Med Mol Imaging
DOI 10.1007/s00259-009-1262-2

ORIGINAL ARTICLE

Quantification of regional myocardial oxygen metabolism in normal pigs using positron emission tomography with injectable ^{15}O-O_2

Takashi Temma · Hidehiro Iida · Takuya Hayashi · Noboru Teramoto · Youichiro Ohta · Nobuyuki Kudomi · Hiroshi Watabe · Hideo Saji · Yasuhiro Magata

Received: 27 April 2009 / Accepted: 10 August 2009

Abstract
Purpose Although ^{15}O-O_2 gas inhalation can provide a reliable and accurate myocardial metabolic rate for oxygen by PET, the spillover from gas volume in the lung distorts the images. Recently, we developed an injectable method in which blood takes up ^{15}O-O_2 from an artificial lung, and this made it possible to estimate oxygen metabolism without the inhalation protocol. In the present study, we evaluated the effectiveness of the injectable ^{15}O-O_2 system in porcine hearts.
Methods PET scans were performed after bolus injection and continuous infusion of injectable ^{15}O-O_2 via a shunt between the femoral artery and the vein in normal pigs. The injection method was compared to the inhalation method. The oxygen extraction fraction (OEF) in the lateral walls of the heart was calculated by a compartmental model in view of the spillover and partial volume effect.
Results A significant decrease of lung radioactivity in PET images was observed compared to the continuous inhalation of ^{15}O-O_2 gas. Furthermore, the injectable ^{15}O-O_2 system provides a measurement of OEF in lateral walls of the heart that is similar to the continuous-inhalation method (0.71 ± 0.036 and 0.72 ± 0.020 for the bolus-injection and continuous-infusion methods, respectively).
Conclusion These results indicate that injectable ^{15}O-O_2 has the potential to evaluate myocardial oxygen metabolism.

Keywords Myocardial oxygen metabolism · PET · Pig · OEF · Injectable ^{15}O-O_2

T. Temma · H. Saji
Department of Patho-Functional Bioanalysis,
Graduate School of Pharmaceutical Sciences, Kyoto University,
Kyoto, Japan

H. Iida · T. Hayashi · N. Teramoto · Y. Ohta · N. Kudomi · H. Watabe
Department of Investigative Radiology,
National Cardiovascular Center Research Institute,
Osaka, Japan

Y. Magata (✉)
Laboratory of Genome Bio-Photonics,
Photon Medical Research Center,
Hamamatsu University School of Medicine,
1-20-1 Handayama,
Hamamatsu 431-3192, Japan
e-mail: magata@hama-med.ac.jp

Introduction

In the myocardium, fatty acid or glucose is used to produce energy by aerobic metabolism. Oxygen is one of the most important substrates closely related to the aerobic metabolism in the TCA cycle; thus, oxygen metabolism should be a direct reflection of myocardial metabolism of these substrates. Therefore, there has been considerable interest in the development of a method to quantify oxygen metabolism in the myocardium.

Recently, ^{11}C-acetate has been used for this purpose [1–5]. ^{11}C-acetate is taken up by the mitochondria and metabolically converted into acetyl-CoA. It then enters the TCA cycle and is transformed to ^{11}C-CO_2, which is cleared rapidly from the myocardium. Thus, the clearance pharmacokinetics reflects oxygen metabolism in the myocardium. However, the quantification of oxygen metabolism using ^{11}C-acetate is quite difficult because of various intermediary compounds.

The use of ^{15}O-O_2 gas inhalation and PET scanning can provide a quantitative myocardial metabolic rate for oxygen ($MMRO_2$) [6, 7]. The tracer kinetic model used is based on that originally proposed to describe the behavior of ^{15}O-O_2 in brain tissue [8, 9]. However, the direct translation of the

Published online: 04 September 2009

compartmental model for the brain to the heart is not permitted, because subtraction for spillover from gas volume in addition to that from the blood pool is needed. A previous study demonstrated that the gas volume can be accurately estimated from the transmission scan data; thus, this technique did not require additional emission scanning for estimating the quantitative gas volume images [6, 7]. However, gaseous radioactivity in the lung during the inhalation of ^{15}O-O_2 gas is too high in comparison to other regions. Subtraction for this contribution is straightforward and accurate using the transmission scan-derived gaseous volume images, but the lung radioactivity degraded image quality in the estimated $MMRO_2$ images.

As an alternative to gas inhalation, we recently developed a method to prepare an injectable form of ^{15}O-O_2. This was accomplished by exposing pre-collected blood to ^{15}O-O_2 gas using a small artificial lung system resulting in a maximum yield of 130 MBq/ml. We demonstrated that cerebral oxygen metabolism could be estimated in normal and ischemic rats using injectable ^{15}O-O_2 [10–12]. This technique has the potential of avoiding the inhalation protocol.

The aim of the present study was therefore to test the feasibility of using the injectable ^{15}O-O_2 oxygen system for estimating myocardial oxygen metabolism in pigs. The injection method was compared to the inhalation method to determine if the injection method resulted in a reduction of lung radioactivity, an improved image quality, a more accurate estimate of myocardial oxygen metabolism, and an improved signal-to-noise ratio.

Materials and methods

Theory

^{15}O-Oxygen was administered by IV injection or inhalation and was carried as ^{15}O-hemoglobin by blood to peripheral tissues including the myocardium, where it was converted to ^{15}O-water (^{15}O-H_2O_{met}) through aerobic metabolism. The increased distribution volume of ^{15}O-H_2O_{met}, represented by the exchangeable water space of tissue, causes delayed removal of radioactivity. This allows the definition of an appropriate model and equations to be derived for the calculation of a regional myocardial metabolic rate for oxygen ($rMMOR_2$) and regional oxygen extraction fraction (rOEF). Previous studies demonstrated that these calculations were similar to those used for estimating cerebral blood flow and oxygen metabolism and require the measurement of regional myocardial blood flow (rMBF) and a correction for spillover of activity from the vascular pools and the pulmonary alveoli [6, 7]. rMBF was measured by the ^{15}O-H_2O injection technique [13]. Activity in the vascular pools of the heart chambers and the lung was evaluated with a conventional measurement of blood volume using ^{15}O-CO, and activity in the pulmonary alveoli was evaluated with an unconventional and indirect measurement of gas volume obtained from the transmission scan. Furthermore, the existence of recirculating ^{15}O-H_2O_{met} in the blood freely accessible to the myocardium was taken into consideration.

The differential equation describing the myocardial kinetics after administration of ^{15}O-O_2 can be written as follows:

$$\frac{dC^{myo}(t)}{dt} = OEF \cdot f \cdot A_o(t) + f \cdot A_w(t) - \left(\frac{f}{p} + \lambda\right) C^{myo}(t) \quad (1)$$

where $C^{myo}(t)$ designates the true radioactivity concentration in the myocardium at time t, f is myocardial blood flow, $A_O(t)$ is the ^{15}O-O_2 radioactivity concentration in arterial blood, $A_W(t)$ is the ^{15}O-H_2O radioactivity concentration in arterial blood, p is the myocardium/blood partition coefficient of water, and λ is the physical decay constant of O-15.

Solving Eq. (1) in terms of $C^{myo}(t)$ gives:

$$C^{myo}(t) = OEF \cdot f \cdot A_o(t) * e^{-\left(\frac{f}{p}+\lambda\right)\cdot t} + f \cdot A_w(t) * e^{-\left(\frac{f}{p}+\lambda\right)\cdot t} \quad (2)$$

where the asterisk denotes the convolution integral. During steady-state conditions under the continuous administration of ^{15}O-O_2, the following relationship holds:

$$C^{myo} = \frac{OEF \cdot f \cdot A_o + f \cdot A_w}{\left(\frac{f}{p} + \lambda\right)} \quad (3)$$

In the actual PET studies, the spillover from vascular pools and pulmonary alveoli and the partial volume effect should be taken into consideration [14]. Then, the measured radioactivity concentration in the region of interest (ROI) in the myocardium ($R^{myo}(t)$) can be expressed as:

$$\begin{aligned} R^{myo}(t) = {} & \alpha \cdot C^{myo}(t) \\ & + (V_B^{myo} \cdot A_t(t) - \alpha \cdot F_{Vein} \cdot OEF \cdot A_o(t) - \alpha \cdot F_{Vein} \cdot A_w(t)) \\ & + V_G^{myo} \cdot C_{gas}(t) \end{aligned} \quad (4)$$

where α denotes the myocardial tissue fraction, V_B^{myo} is the myocardial blood volume, $A_t(t)$ is the total O-15 radioactivity concentration in arterial blood, F_{vein} is the microscopic venous blood volume, V_G^{myo} is the gas volume in the myocardial ROI and $C_{gas}(t)$ is the O-15 radioactivity concentration in V_G^{myo}.

With the bolus injection or infusion methods using an artificial lung system, the radioactivity in the pulmonary alveoli is expected to be negligible in comparison with the inhalation method. Thus, Eq. (4) can be converted to:

$$R^{myo}(t) = \alpha \cdot C^{myo}(t) + (V_B^{myo} \cdot A_t(t) - \alpha \cdot F_{Vein} \cdot OEF \cdot A_o(t) - \alpha \cdot F_{Vein} \cdot A_w(t)) \quad (5)$$

Subjects

In this study, four healthy miniature pigs (22–30 kg) were used. The pigs were anesthetized by IM injection of ketamine and xylazine followed by continuous infusion of propofol (5 mg/kg/h). The animals were then placed in the supine position on the bed of the PET scanner. All experimental procedures were approved by the local animal welfare committee.

Injectable ^{15}O-O_2 preparation

In the "injection" study, injectable ^{15}O-O_2 was used. Injectable ^{15}O-O_2 was prepared as described previously [10–12]. In brief, part of an infusion line kit (Terumo Corporation, Tokyo, Japan) and an artificial lung 18 cm in length (Senko Medical Instrument Mfg Co. Ltd., Tokyo, Japan) were connected using silicone tubing to make a closed system. Then, venous blood collected from a pig, which was used in the following PET studies, was added to the system and circulated (100 ml/min) by a peristaltic pump, followed by introduction of ^{15}O–O_2 gas (~7,000 MBq/min/433 ml) into the artificial lung for 15 min to prepare injectable ^{15}O-O_2 (5.6–60.7 MBq/ml).

In the "continuous infusion" study, the left femoral artery and right femoral vein were both cannulated. The two cannulas from the artery and the vein were connected to the opposite sides of an artificial lung to create a femoral shunt. The blood flow in the shunt was aided by a peristaltic pump (30–50 ml/min). ^{15}O-O_2 gas (~7,000 MBq/min/433 ml) was continuously introduced into the artificial lung.

PET protocol (Fig. 1)

The PET scanner was an ECAT EXACT HR (CTI/Siemens) [15], which has an imaging field of view (FOV) of 55 cm in diameter and 15 cm in axial length. The spatial resolution of the scanner is 5.8 mm in full width at half maximum at the center of the FOV.

After obtaining a 20-min transmission scan for attenuation correction and gas volume estimation, the blood pool image was obtained with a 4-min PET scan after the pigs inhaled 2.7 GBq ^{15}O-CO for 30 s. Arterial blood samples were taken every minute during the ^{15}O-CO scanning, and

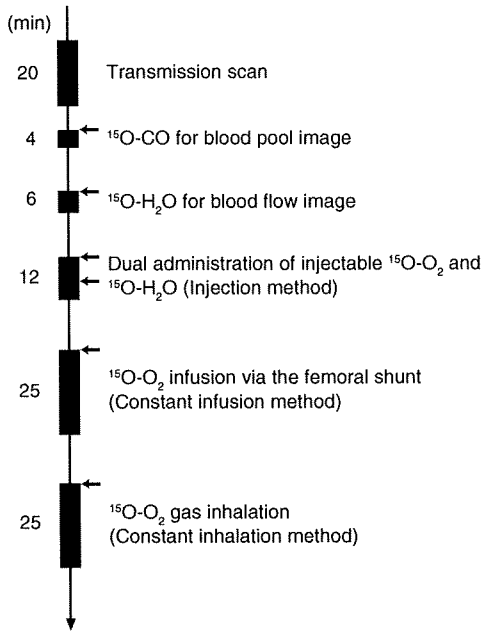

Fig. 1 Outline of the PET imaging study. The interval between scans was more than 15 min to allow for physical decay of O-15 radioactivity to background levels

the radioactivity concentration in the whole blood was measured with a NaI well-type scintillation counter calibrated against the PET scanner. Subsequently, ^{15}O-water was injected into the right femoral vein for 30 s at an infusion rate of 10 ml/min (injected radioactivity was about 1.11 GBq). Immediately after injection of ^{15}O-water, 26 dynamic frames (12×5 s, 8×15 s and 6×30 s) of PET data were acquired for 6 min.

Furthermore, two PET scans were successively performed after the IV injection of ^{15}O-O_2 (5.6–60.7 MBq/ml) for 30 s at an injection rate of 20–80 ml/min for the "injection" study, and by the continuous ^{15}O-O_2 gas infusion through the artificial lung in the femoral shunt for the "continuous infusion" study. In the "injection" study, 52 dynamic frames (12×5 s, 8×15 s, 6×30 s, 12×5 s, 8×15 s and 6×30 s) of PET data were acquired for 12 min, and 1.11 GBq of ^{15}O-water was injected IV for 30 s at 10 ml/min starting at 6 min after the administration of IV ^{15}O-O_2 according to the dual administration protocol we developed previously [16]. In the "continuous infusion" study, 26 dynamic frames (10×30 s, 5×60 s, 1×600 s and 10×30 s) were acquired for 25 min, and the 600-s frame was used for steady-state analysis.

Another PET scan was performed by ^{15}O-O_2 gas inhalation in one of the four pigs in the same protocol as the "continuous infusion" study. This was the "continuous inhalation" study. The interval between scans was more

than 15 min to allow for physical decay of O-15 radioactivity to background levels. All acquisitions were obtained in the two-dimensional mode (septa extended).

Data analysis

A filtered back-projection algorithm with a 6-mm Gaussian filter was used for image reconstruction. The reconstructed images had a matrix size of 128 × 128 × 47 and a voxel size of 1.84 × 1.84 × 3.38 mm, and all image data sets were resliced into short-axis images across the left ventricle [13].

Myocardial blood flow

rMBF was calculated from the injection of ^{15}O-H_2O by fitting the myocardial and arterial time-activity curve data to a single-tissue-compartment model that implemented corrections for partial-volume effects by introducing the tissue fraction. In addition, the model was corrected for spillover from the left ventricular (LV) chamber into the myocardial ROI by introducing the arterial blood volume [13]. In these experiments, the time-activity curves generated from large ROIs placed in the LV chamber were used as the input function.

Regional oxygen extraction fraction

In the "injection" study, rOEF was calculated according to Eqs. (2) and (5). In these formulations, F_{vein} was assumed to be 0.10 ml/g tissue and p was fixed at 0.90 ml/g. The blood volume image obtained from the ^{15}O-CO scan was used for the determination of V_B^{myo}. The value of $A_t(t)$ was obtained from the LV radioactivity concentration measured from the PET data set with small LV ROIs to minimize spillover from the myocardium. The calculation for the estimation of recirculating ^{15}O-H_2O was performed as previously described [16]. For the "continuous infusion" and "continuous inhalation" studies, in which a 600-s frame was regarded as steady-state, Eqs. (3) and (5) or Eqs. (3) and (4) were used for calculating rOEF, respectively.

Results

Table 1 summarizes the conditions of animals during the PET studies. The parameters were all within the physiologic range.

Figure 2 demonstrates the dynamic images obtained in the "injection", "continuous infusion", and "continuous inhalation" studies. With the injection and continuous-infusion methods, the right ventricle on the left side and the vena cava on the lower side were well delineated, whereas the left ventricle was moderately shown on the right side. The 16th frame (600~1,200 s after the initiation), which was used for steady-state analysis with the continuous-infusion method, was visibly distinct compared with all of the frames obtained with the injection method. However, with the continuous-inhalation method, neither ventricle could be depicted because of high radioactivity in the lung on the right and lower-side images.

The radioactivity in the blood pool obtained by ^{15}O-CO PET (Fig. 3g) and the gaseous volume estimated by inverse transmission data (Fig. 3h) were subtracted from the raw PET images (16th frame) with the continuous-inhalation and continuous-infusion methods, respectively (Fig. 3c and f). Both methods clearly delineated the myocardium after subtraction in comparison to the blood flow image (Fig. 3i). However, the continuous-inhalation method showed salient radioactivity on the lateral wall (Fig. 3c), whereas the continuous-infusion method showed only modest radioactivity in the myocardium (Fig. 3f). It is also notable that there was considerable radioactivity in the right ventricle with the continuous-infusion method even after the subtraction (Fig. 3f).

To further examine the differences between the continuous-infusion and continuous-inhalation methods, time-radioactivity curves during the PET scans were taken from four ROIs: the left ventricle (LV), right ventricle (RV), myocardium (Myo), and lung (Fig. 4). At the steady-state frame (600~1,200 s), the continuous-infusion method showed higher radioactivity in the RV and LV than in the myocardium (Fig. 4a), whereas the radioactivity of these regions was similar with the continuous-inhalation method (Fig. 4b). The radioactivity in LV was about two-thirds of that in RV in Fig. 4a, indicating that measurable radioactivity was excreted through the lung even after the femoral administration of ^{15}O-O_2. The lung excretion was also observed on the blood-subtracted image (Fig. 3e). Actually, there was significant radioactivity in the lung (Fig. 4a), although that was the lowest among the four ROIs. In contrast, the radioactivity in the myocardium was the lowest among the four ROIs with the continuous-inhalation method

Table 1 Physiological parameters of pigs during the PET studies

	pH	pCO_2 (mmHg)	pO_2 (mmHg)	tHb (g/dl)	O_2Sat (%)	HR (bpm)	BP (mmHg)	
							Diastolic	Systolic
Average	7.46	40.3	125.8	12.8	97.7	85	97.8	125.2
SD	0.032	2.51	16.69	1.30	1.83	19.5	10.4	19.3

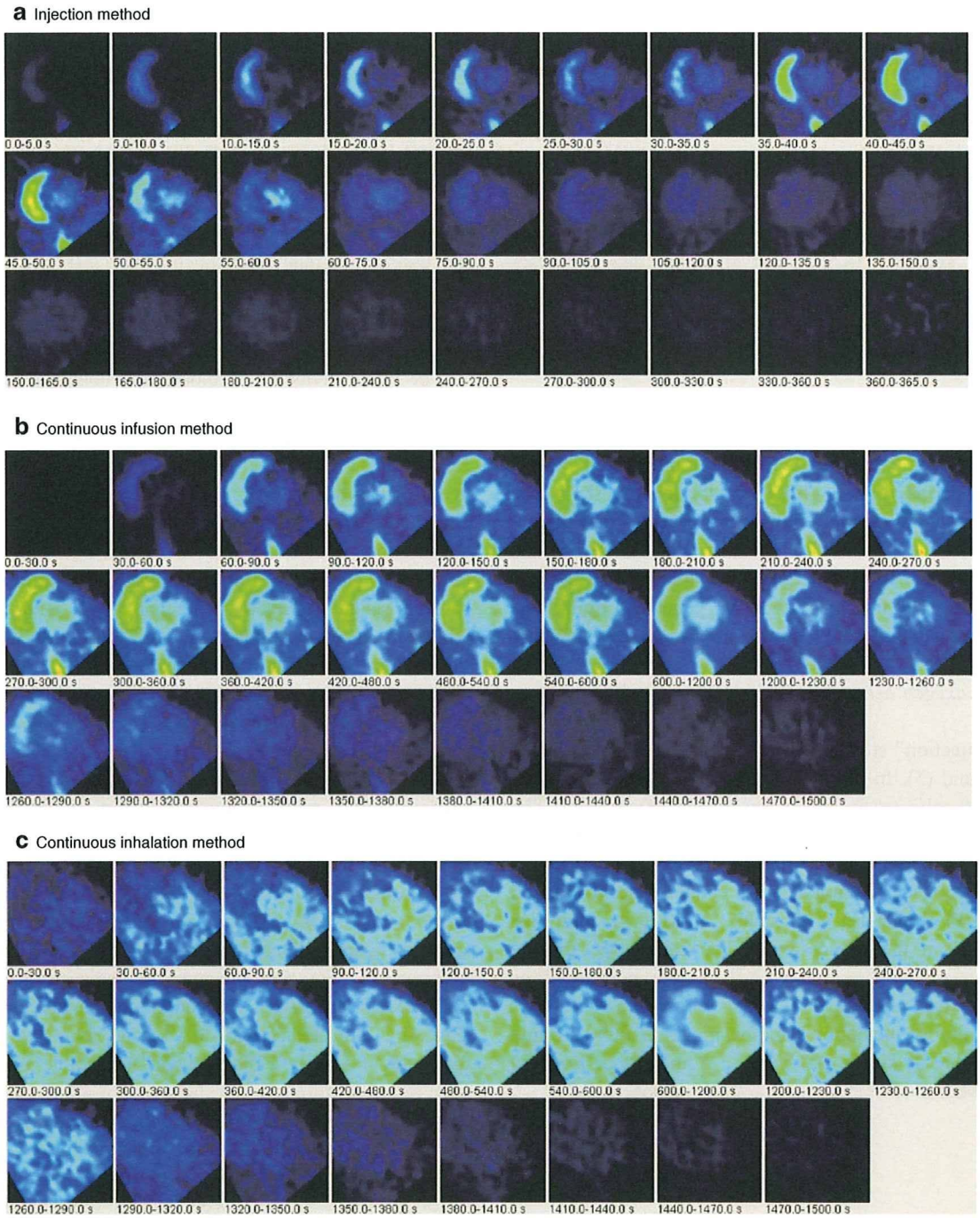

Fig. 2 PET images obtained in (**a**) the injection method, (**b**) the continuous-infusion method with injectable ^{15}O-O_2, and (**c**) the continuous-inhalation method with ^{15}O-O_2 gas

(Fig. 4b). The heart-to-lung radioactivity ratios were calculated from Fig. 4 for the quantitative estimation of image quality; the continuous-infusion method provided a ratio of 1.38±0.24, whereas the ratio was less than one with the continuous-inhalation method.

Table 2 shows the quantitative OEF values in the lateral wall obtained by the injection, continuous-infusion, and continuous-inhalation methods. These OEF values were consistent among the three methods.

Figure 5 represents the noise equivalent counts (NEC) standardized by the total counts detected by the PET scanner. Although the injection method tended to show rather high values, there was no significant difference between the values obtained by the injection and

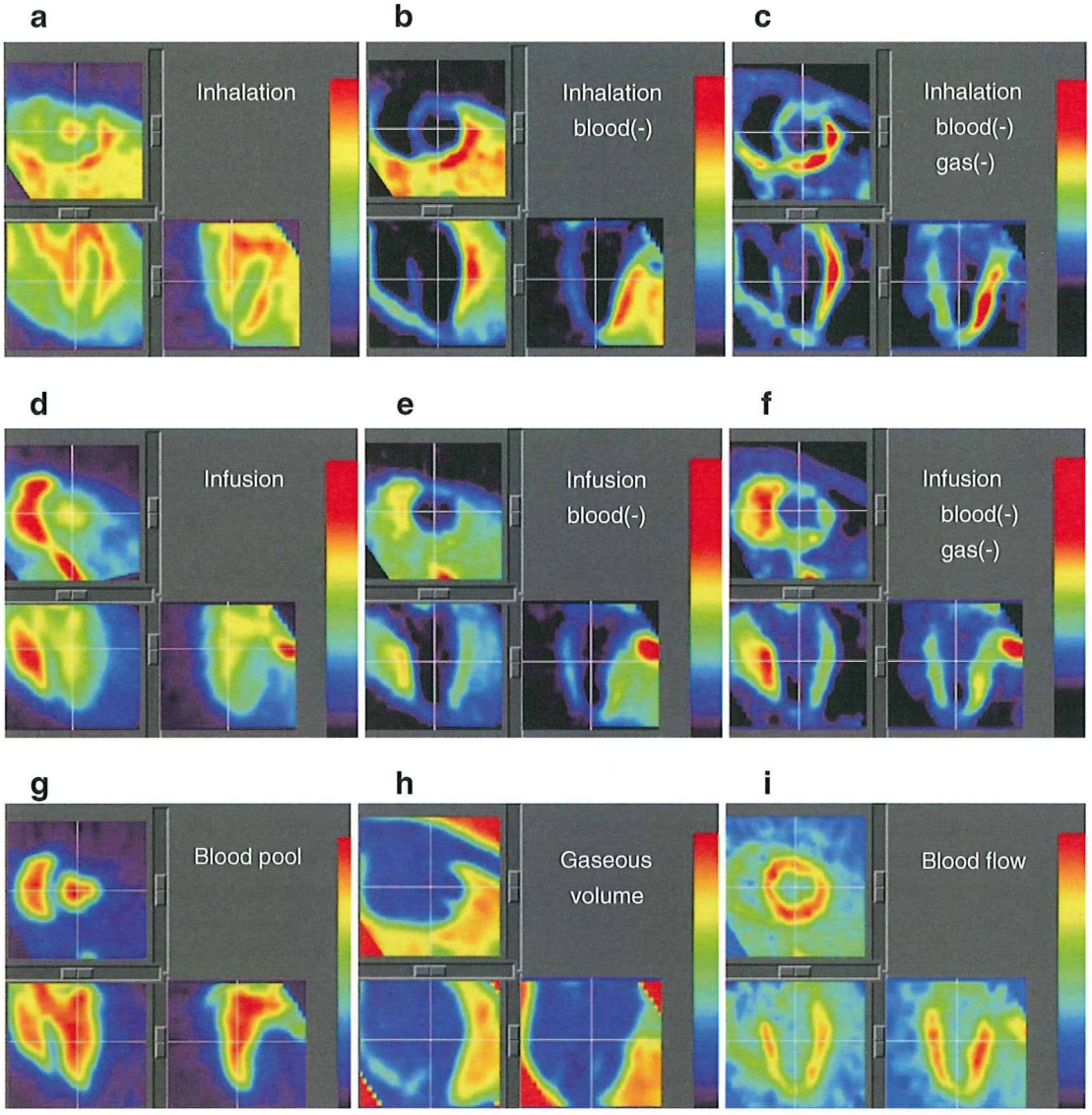

Fig. 3 PET images obtained in the study are shown. The 16th frame (steady-state frames) of the continuous-inhalation method and the continuous-infusion method are shown in (**a**) and (**d**), respectively. The 'blood-subtracted' images shown in (**b**) and (**e**) were created by subtraction of the blood-pool image by ^{15}O-CO (**g**) from (**a**) and (**d**). The 'blood- and gas-subtracted' images shown in (**c**) and (**f**) were created by the successive subtraction of the gaseous image (**h**) from (**b**) and (**e**). The myocardial blood flow image is also shown in (**i**)

continuous-infusion methods as determined by a Mann Whitney *U*-test.

Discussion

In previous studies, we showed the usefulness of the injectable ^{15}O-O_2 system for estimating cerebral oxygen metabolism in small animals such as rats under normal or ischemic conditions [10–12]. Injectable ^{15}O-O_2 replaced the inhalation protocol and radioactive ^{15}O-O_2 was administered via the tail vein. Thus, injectable ^{15}O-O_2 could abolish the artifact from the high radioactivity in the inhalation tube that distorts the PET images, especially in small animals. We considered that the concept could also be utilized in the hearts of large animals. Therefore, in the present study, we tested the feasibility of an injectable ^{15}O-O_2 system for estimating myocardial oxygen metabolism in normal pigs. In addition, since a shunt between the femoral artery and vein can be created in pigs but not in small animals, continuous infusion via the femoral shunt was also performed to achieve a constant and reliable delivery of radioactivity to the heart.

Dynamic PET scans showed a large difference in the radioactivity distribution among the three methods. Since the labeling efficiency to prepare injectable ^{15}O-O_2 was